Study of Radar Signatures of Drones Equipped with Threat Payloads

Samiur Rahman, Duncan A. Robertson, Adam M. Robertson
University of St Andrews; School of Physics and Astronomy
North Haugh, St Andrews, KY16 9SS
UNITED KINGDOM

sr206@st-andrews.ac.uk, dar@st-andrews.ac.uk

Mark A. Govoni
Us Army Research Laboratory
ATTN: FCDD-RLS, Adelphi, MD 20783-1138
UNITED STATES OF AMERICA

ABSTRACT

Commercial or customised drones with the ability to carry payloads have the potential to cause security threats so the need to accurately detect and identify them with suitable sensors has increased in recent times. Radar sensors are well capable of detecting and classifying a drone by using the unique signatures produced from both the stationary and rotating parts of the target. In this study we have examined the radar signatures of drones carrying different types of payloads which simulate the following three hazardous scenarios: 1) liquid spray, 2) Inertial forces simulating a gun recoil effect, and 3) heavy payloads. The main objective was to model the radar signatures of these scenarios and analyse the characteristic signatures. Two radars, operating at 24 GHz and 94 GHz, have been used to collect data to validate the modelling. The results of the study demonstrate that the payloads produce unique radar return signals, mainly in the Doppler domain, which can be used for robust classification.

1.0 INTRODUCTION

The business sector is forecasting that the global market size of small drones will reach $22.55 billion by 2026, with a compound annual growth rate of 15.92% [1]. Along with the obvious socio-economic benefits, this proliferation is also significantly increasing the security threats related to drones [2]. To tackle the security challenge, it is of great interest to understand the discriminating signatures presented by drones to various sensors. Due to all-weather operability and longer range coverage, radar is one of the primary sensors to detect and classify a drone. In [3][4], the theoretical framework has been laid out for analysing the radar micro-Doppler signature of a drone. Based on micro-Doppler, a number of research works have proposed methods to classify drones [5][6].

Whilst there has been a large quantity of research published in recent years on drone detection by radar, not much work has been reported regarding the radar signatures of drones carrying payloads. In [7] changes in drone micro-Doppler signatures were studied with and without payload, demonstrating the capability of radar to detect the presence of a payload. However, more controlled experimental data analysis is required to ensure that the drone signature with payload corresponds only to the payload and nothing else (e.g. wind). According to our knowledge, there is no available literature reporting on radar signatures of drones carrying a liquid spray payload or an inertial payload generating a recoil effect (e.g. a gun).

In this study, our goal is to report on the different payload effects on the radar signatures of drones which we deem to be quite timely and very relevant to the military and security sectors. We have performed modelling

Figure 1: Crop spray drone hovering. The liquid spray is seen below the drone.

of scenarios with different payloads to gain basic understanding of how their presence modulates the radar return signal. The three different scenarios we have considered are as follows:

1. Drone equipped with liquid spray payload
2. Drone equipped with simulated recoil
3. Drone equipped with heavy payload

We have also performed experimental trials to validate the simulation results. Radar systems at 24 [8] and 94 GHz [9] have been used to gather experimental data of drones in flight for the above three scenarios. Our overall data analysis shows that radar sensors are able to obtain distinctive signatures of drones carrying these specific payloads, especially at millimetre-wave frequencies.

2.0 LIQUID SPRAY PAYLOAD

The danger of drones being used for carrying chemical/biological weapons has become very tangible in recent times [10]. In this study, we have modelled the liquid spray radar backscatter at different frequencies, assuming water as the liquid. A crop spray drone [11] was procured for this study to obtain real data – figure 1. The droplet parameters used during modelling are according to the manufacturer's specification.

The liquid droplet sizes (diameters) vary from 50-200 µm. If the maximum value is considered (200 µm) and spherical droplets are assumed, the ratio of the sphere's circumference to the wavelength $2\pi a/\lambda$ becomes 0.19 at 94 GHz and 0.05 at 24 GHz. In both cases, $2\pi a/\lambda << 1$, so the droplet sizes are quite small compared to the wavelengths which makes the Rayleigh approximation appropriate for the volume reflectivity calculation. The volume backscatter coefficient, η, for an ensemble of particles of diameter D can be calculated as follows [12],

$$\eta = \frac{\pi^5 f^4}{c^4} |K|^2 \sum D^6 N \, dD \qquad (1)$$

where f and c are the operating frequency and the speed of light respectively, $|K|$ is the refractive index factor equal to (m^2-1 / m^2+2), m being the complex refractive index of the water drops. Here, $m=\sqrt{\varepsilon}$ and ε is the permittivity. This value is calculated for 20 °C by using the Debye formula [13]. Values obtained for $|K|^2$ at 10, 24 and 94 GHz are 0.92, 0.88 and 0.68 respectively. N is the number of particles in the size interval D to $D+dD$. The summation part of the equation is the radar reflectivity factor Z [12],

$$Z = \sum D^6 N \, dD \qquad (2)$$

Z is calculated by summing over different values of D ranging from 50-200 µm with *dD* being 10 µm. *N* is obtained from the total volume of atomised liquid divided by the average droplet volume. For our crop spraying drone with a 5 litre tank we assume the average droplet diameter to be 125 µm and obtain the following value for radar reflectivity factor: Z = 0.6614 mm^6/m^3 and dBZ = 10*log(Z) = -1.8 dBZ (note this is independent of frequency). From this the volume backscatter coefficient η is calculated to be 1.77e-10, 7.3e-09 and 1.3e-06 m^2/m^3 at 10, 24 and 94 GHz respectively.

This validates the assumption that W-band radar will be better than lower frequencies for liquid spray backscatter signature analysis as the backscatter coefficient is substantially higher than at X- and K-bands.

In meteorological radar one calculates the RCS as the product of the volume backscatter coefficient and the range cell volume. That approach is not appropriate in this case as the liquid spray underneath the drone will have a fairly limited volume and will not necessarily fill the beam at all ranges. Hence, we have calculated the fraction of the range cell occupied by the spray volume as a function of range as follows.

The volume of the radar range cell is calculated assuming it has the shape of a frustum (truncated cone) with the volume $V = (\pi/4)\,(R\theta)\,(R\varphi)\,(c/2B)$. Here, θ and φ are the azimuth and elevation one-way 3dB beam widths respectively, R is the range and B is the signal bandwidth. During simulation we make the simple assumption that the volume of the spray emanating from the 4 nozzles on the drone forms a vertical cylinder of fixed diameter and height. We assume the horizontal diameter of the spray volume matches that of the diameter of the drone which is 1.2 m. We assume that the spray volume is uniform over a vertical height of 5

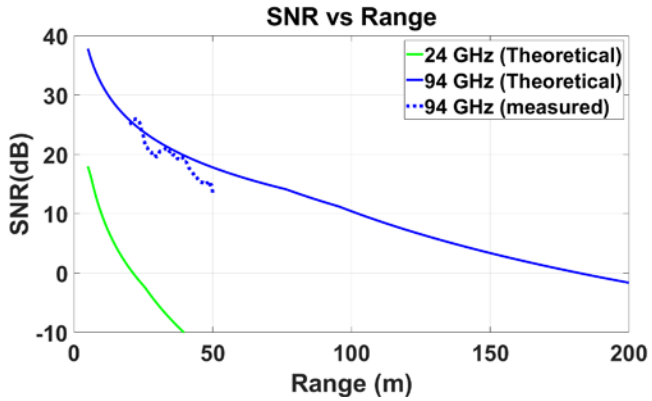

Figure 2: Volume occupied by liquid spray within each range cell and associated RCS at 94 GHz.

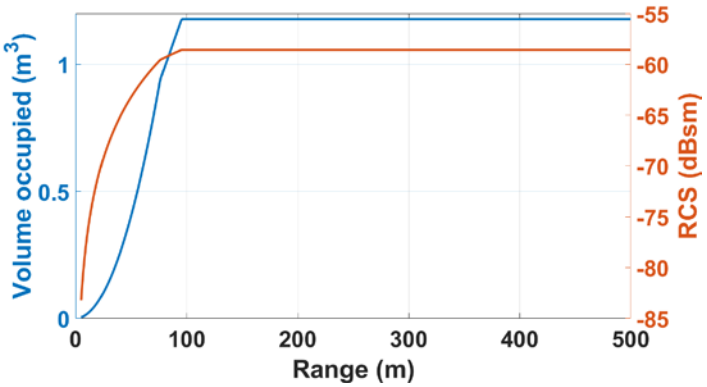

Figure 3: SNR versus range showing theoretical curves for the 94 GHz and 24 GHz radars and the measured data at 94 GHz.

m, below which the spray has dispersed. This is the recommended operating height when delivering a consistent amount of crop spray. These values are used along with the antenna beamwidth of the existing radars to model the volume occupied at each range bin. Using the volumetric values the SNR can be calculated according to the radar parameters.

Experimental data was obtained using 24 [8] and 94 GHz [9] Frequency Modulated Continuous Wave (FMCW) radars. For the 94 GHz radar (T-220) $\theta = 0.9°$ and $\varphi = 3°$ and for the 24 GHz radar $\theta = \varphi = 11.2°$. An upper limit has been put on the arc length $R\theta$ (1.2 m) when calculating the volume V. In terms of the elevation axis, the assumed 5 m vertical extent of the spray volume places an upper limit on how much of the elevation axis is filled as range increases and this has been used during the calculation of $R\varphi$. It should be noted that θ and φ are in radians when calculating the arc lengths. We can thus calculate the volume within the radar beam occupied by spray as a function of range and this is shown in figure 2. It can be seen that at short ranges (below ~100 m) the spray fills the radar range cell as the beam size is smaller than the spray extent but at greater ranges the spray volume remains constant and is smaller than the range cell. For a given volume backscatter coefficient, η, the target radar cross section, $\sigma = \eta V$, is also plotted in figure 2 for 94 GHz. It can be seen that at ranges in excess of ~100 m, the RCS value of the liquid spray is around -58 dBsm. This is expected to be approximately 40 dB lower than the return signal strength from the drone itself [14]. Using the volumetric values, the SNR can be calculated according to the radar parameters.

In figure 3, the theoretical SNR is plotted and the measured values [15] are overlaid. The agreement between the theoretical and measured values is clearly observed. The results confirm that (i) liquid spray is undetectable using the 24 GHz radar (SNR < 0 dB) for all but the shortest ranges, and (ii) liquid spray is well detected by the 94 GHz T-220 radar with detection possible up to 100 to 150 m with good agreement between experiment and modelling. It is also observed from the theoretical SNR at 94 GHz in figure 3 that around 100 m range, the $1/R^2$ behaviour typical of beam filling meteorological radar targets changes to the $1/R^4$ behaviour of finite sized targets which are smaller than the range cell (sub-beamwidth).

3.0 SIMULATED RECOIL

This section aims to investigate whether inertial forces inherited from a dynamic payload impart characteristic changes on the drone's radar signature which can be used to identify the particular payload. The hypothesis is that a drone reacting to some payload-induced inertial force is likely to show a characteristic change in its kinematic behaviour and position as it jerks about then re-stabilises. This could be revealed in high range resolution profiles (HRRPs) or the RCS and Doppler signatures could exhibit some unique modulation which may be identifiable. To our knowledge, there has been no prior work addressing this scenario.

The objective is to measure the displacement due to gun recoil. This can be calculated by measuring the recoil force:

$$\int F dt = m_f v_f \tag{3}$$

Here, m_f is the firearm mass and v_f is the firearm velocity. Then using the conservation of momentum principle, the displacement of the firearm can be calculated as

$$\Delta d_f = v_f \Delta t \tag{4}$$

where Δt is the time resolution. During modelling, this displacement over impulse time is implemented to observe the effect on the micro-Doppler response.

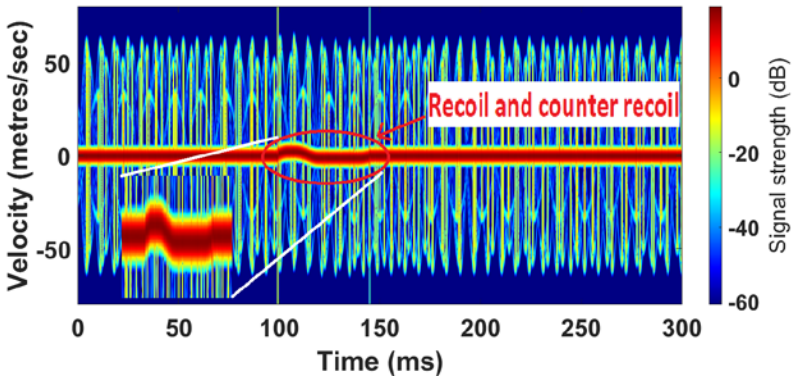

Figure 4: Simulated micro-Doppler signature of a quadcopter showing recoil-counter recoil effect on the bulk Doppler.

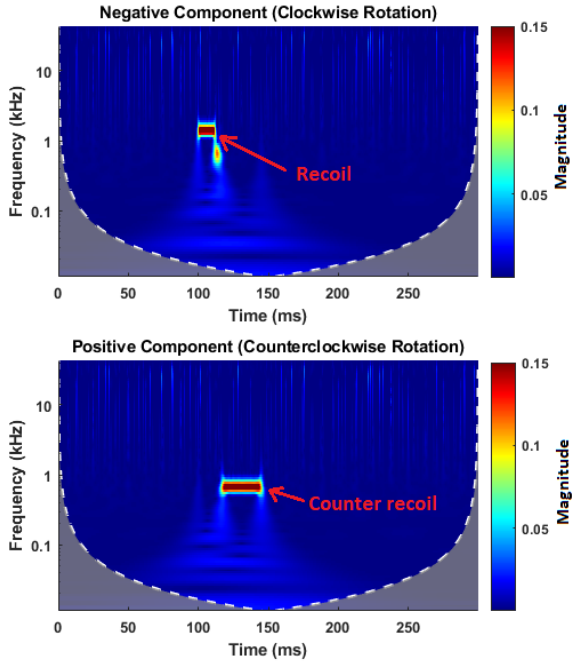

Figure 5: Simulated scalogram plot of a quadcopter showing the recoil-counter recoil effect on the bulk Doppler.

Parameters for gun displacement and impulse response time have been obtained from the experimental trial performed in [16]. In that work, recoil characteristics were measured by applying absorptive pads to the back of the stock carriage which transmitted the force to a cantilevered lever connected to a load-cell. Two types of hardness of hemispherical pad were studied. The more compliant, referred to as 'Soft-Hemi' is a 30 Duro model from Sorbothane, Inc., while the less compliant (70 Duro model) is labelled 'Hard Hemi', The values for the less compliant 'Soft Hemi Foam' model are used here as a representative estimate. Change in range during the impulse time is implemented to observe the effect on the micro-Doppler response.

Modelling of recoil force is applied to the simulated micro-Doppler signature of a quadcopter with fuselage and 4 propeller blades rotating at different rates. The propeller blade signals are assigned to be ~30 dB lower than the return from the fuselage, consistent with the observations in [17]. The rotation rates have been

assigned randomly ranging from 50-100 Hz (typical values for a quadcopter whilst hovering). The sampling rate is 100 kHz to unambiguously resolve the blade flashes. It is anticipated that the rotation rate of the blades will change due to the inertial force but we have refrained from considering this as a potential signature as it cannot be solely attributed to the recoil effect. Instead, we hypothesise that the perturbation will produce a discernible bulk Doppler signature. This micro-Doppler model was modified to simulate a recoil being applied to the quadcopter in the radial direction. The displacement imposed to simulate recoil was according to the 'Soft Hemi Foam' model curve [16]. Here, the initial recoil displacement is around 4 cm away from the radar in the first 0.015 s. Then there is a very small steady state period between 0.015-0.017 s due to inertia. Finally, the counter-recoil occurs from 0.017-0.045 s, and it returns back to the original position. Figure 5 shows the simulated spectrogram pertaining to the recoil effect. The spectrogram is generated by using a Gaussian window with a width factor of 16 and with a 95% overlap, providing good temporal resolution. The recoil-counter recoil effect is noticeable on the bulk Doppler of the fuselage but not particularly evident on the propeller micro-Doppler. Along with spectrogram generation using Short Time Fourier Transform (STFT), wavelet transformation analysis is also performed using the Wavelet Toolbox in MATLAB®. Since different shapes of wavelets can be used as opposed to the sine wave based STFT, wavelet transformation is very useful in analysing short impulses within a signal [18]. Continuous Wavelet Transform (CWT) is performed on the same simulated complex time series data. The CWT scalogram is generated using the commonly chosen Morse wavelet, which is useful for analysing local discontinuities, where the symmetry parameter is defined as 3 and the time-bandwidth product is 60. The sampling rate is the same as it was for the spectrogram (100 kHz). The minimum and maximum scales are generated automatically with respect to the energy distribution in both frequency and time domain. The scale-to-frequency conversion is done in terms of the sampling frequency. In figure 5, the recoil effect is seen in the anti-analytic part (negative component) of the CWT and the counter-recoil effect is seen on the analytic part (positive component). This is because during recoil the drone is moving away from the radar, corresponding to negative Doppler or positive velocity. The scalograms in figure 5 are displayed by suppressing the areas outside the cone of influence (where edge effects occur). It can be seen in the scalograms that the amplitude is higher where the impulse has occurred, illustrating the benefit of using the wavelet transformation because during recoil the drone is moving away from the radar, corresponding to negative Doppler or positive velocity. The scalograms in figure 5 are displayed by suppressing the areas outside the cone of influence (where edge effects occur). It can be seen in the scalograms that the amplitude is higher where the impulse has occurred, illustrating the benefit of using the wavelet transformation technique to analyse the recoil effect due to inertial forces. The faint vertical lines at higher frequencies in the scalograms in figure 5 correspond to the blade flashes.

To validate the modelling we collected experimental data on a DJI Phantom 3 Standard drone subject to a sudden inertial force. As it was not possible to use a gun due to various logistical reasons, we imparted impulses to the drone by pulling it sharply several times using a wire. The wire was few metres long with one end attached to the main body of the drone and the other end to the tip of a wooden pole. This pole was held upwards and by sharply pulling it backwards, impulse was generated, thus simulating the recoil effect. Due to the drone's internal stabilisation mechanism, it then returned back to its previous position, which is the counter recoil.

The recoil effect can clearly be seen in figure 6 and is qualitatively consistent with the modelled results in figure 5. In figure 7, the force-time and velocity-time profiles derived from the 4th impulse from figure 6 are plotted. Note the counter-recoil duration is about four times longer than the recoil time as the flight controller works to stabilise the drone.

The collected data has then been analysed to calculate the corresponding force and recoil velocity. We have then calculated various parameters as follows:- impulse time: 338.1 ms, peak velocity: 1.90 m/s, peak force:

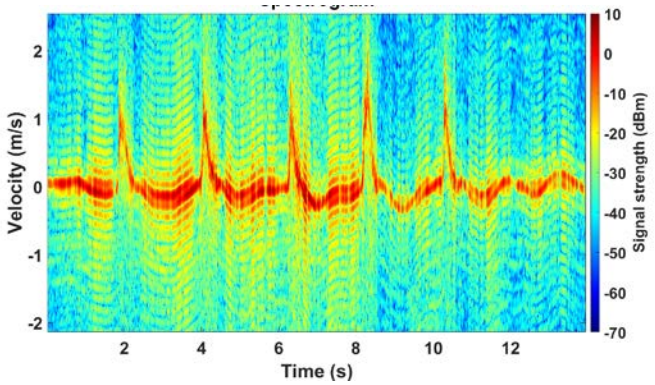

Figure 6: Experimental setup measured 94 GHz FMCW-Doppler spectrogram of drone subject to 5 impulse events, showing the effect of recoil and subsequent counter-recoil.

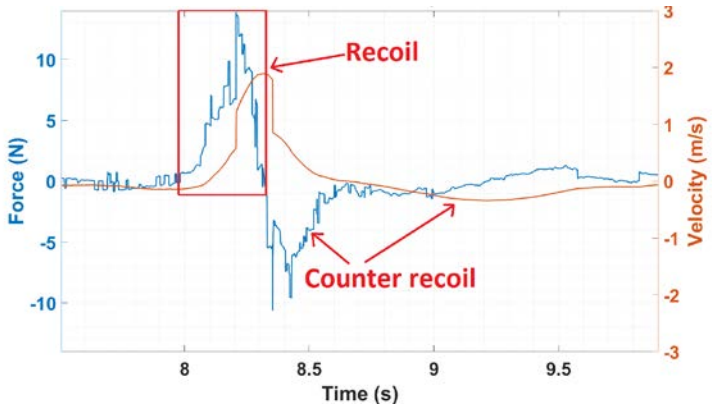

Figure 7: Close up of impulse #4 force-time and velocity-time profiles showing recoil and counter-recoil regimes.

13.90 N, recoil impulse: 1.71 N.s and recoil energy: 2.17 J. These values are comparable to the recoil properties of a Glock 22 pistol (weight 0.65 kg) firing a 9 mm parabellum [19], when it is considered to be attached to a DJI Phantom which weighs 1.2 kg. By taking the added weight into account, recoil velocity would be 1.89 m/s and the recoil energy would be 3.3 J. It can be concluded that the values obtained from the experimental trial are within an appropriate order of magnitude. This confirms that a radar sensor should be capable of detecting the signature of the recoil of a drone-mounted gun.

4.0 HEAVY PAYLOAD

In this scenario, our hypothesis is that the drone propeller rotation rate will increase with an attached payload as extra thrust is delivered to compensate for the added weight, after [7]. This suggests that using a CW radar would be beneficial, as it is easier to unambiguously sample the Doppler shift produced by the fast rotating blades. The rotation rate can be then calculated from the generated spectrogram. One problem is that since there are signal returns from multiple rotors, it is not straightforward to determine accurately the rotation rate from measured radar data. The tip velocity is also difficult to determine as it is heavily aspect angle dependent. We have proposed two methods to determine the dominant rotation rate: (i) generating the cadence velocity diagram of the time series data continuously, and (ii) applying singular value decomposition (SVD) to the spectrogram matrix.

For this study we obtained a customised drone (DJI S900, weight 3.3 kg) which can carry payloads up to 2.5 kg that can be released remotely. Experimentally collected 94 GHz CW spectrograms confirm that there is an increase in the rotation rate with the addition of a payload. The blade flashes from the spectrograms

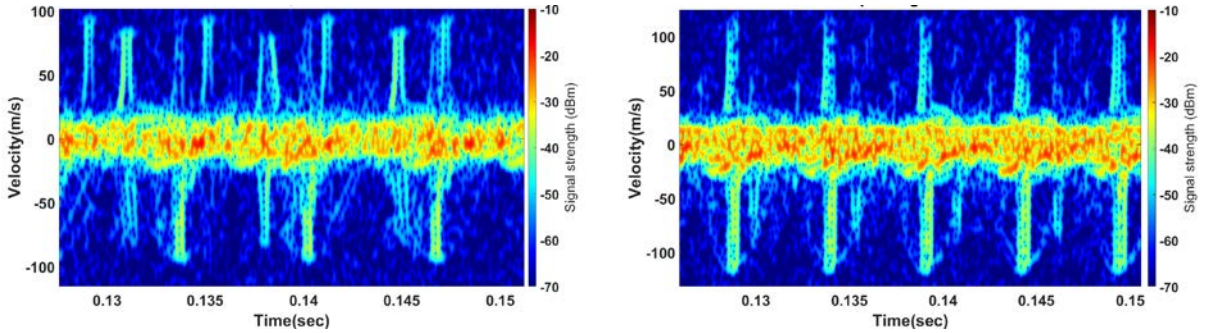

Figure 8: Measured 94 GHz CW spectrogram of S900 hovering without payload (left) and with 2.5 kg payload (right) showing an increase in tip velocity with payload.

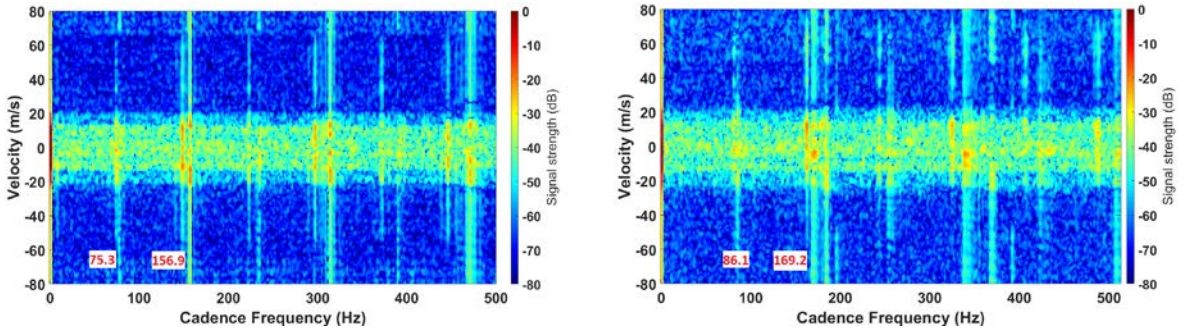

Figure 9: 94 GHz cadence velocity diagrams of S900 hovering without payload (left) and with 2.5 kg payload (right) showing an increase in dominant rotational frequency with payload.

provide information regarding the blade tip velocities. As can be seen in figure 8, without payload, the tip velocity is ~100 ms^{-1}, whereas with the 2.5 kg payload, the rotation rate becomes ~120 ms^{-1}, a 20% increase in velocity. This phenomenon can be used to detect the presence of a payload while the drone is continuously measured. However, as mentioned above, it is unrealistic to expect that the micro-Doppler signatures will always be this prominent, which was also confirmed from the experimental trial results.

Generating the cadence velocity plots from the raw data gives a better visualisation of the dominant frequencies within a Doppler signature modulated by the returns from multiple propeller blades. Figure 9 shows an example of the cadence velocity diagram with and without the 2.5 kg payload where the radar return signal strength from the propeller blades were comparatively lower. In figure 9 (left), the first two prominent frequency values are ~75 and ~157 Hz for an unladen drone.

With the payload attached, the values get shifted to the right as seen in the figure 9 (right). This is obviously due to the overall increase in the rotation rate. It should be noted that in the cadence velocity diagrams, the vertical lines appearing at higher frequencies are mainly harmonics of the lower frequencies.

To make the process automated for a real-time application, we also propose a processing step involving SVD. The advantage then is the ability to obtain a single numerical value corresponding to the dominant frequency.

Figure 10 shows all the steps of the process. A long time series data is segmented and STFT is applied to generate spectrograms of those segments. Then SVD is performed on the spectrograms. Only the V matrix data is selected which corresponds to temporal features (Doppler periodicity). After performing the Fourier transformation of that, the first peak value is selected which is defined as the dominant rotational frequency. A threshold needs to be set to select the first peak, which will determine the sensitivity and false alarm rate. Figure 11 shows an example result of the whole process obtained from the experimental trial data,

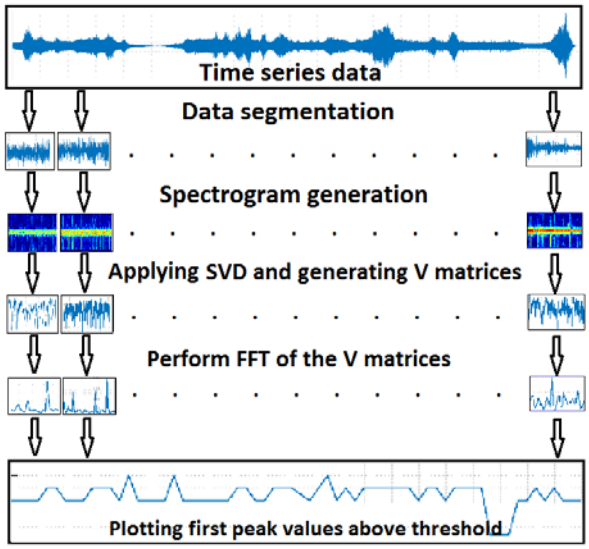

Figure 10: Flow diagram to determine the dominant Doppler frequency from CW radar data.

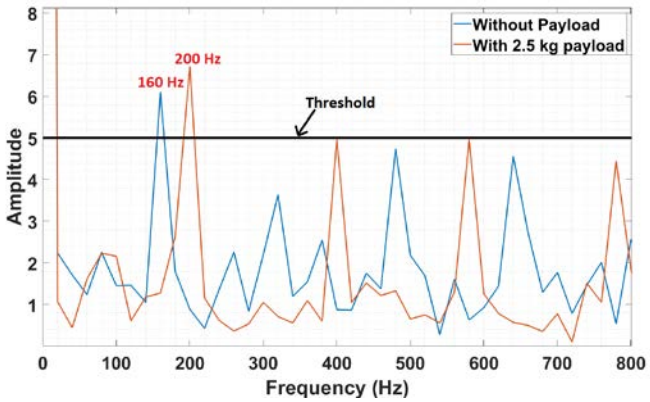

Figure 11: Example result of the SVD based dominant frequency determination process showing frequency increase due to attached payload, at 94 GHz.

demonstrating the frequency shift with presence of the payload.

To test the robustness of the method, experimental data was collected for three more weights (1, 1.6 and 2 kg) using the 94 GHz radar. In each case, the data was taken while the drone was hovering with the payload attached and then releasing it after a while. In figure 12 it is seen that the dominant frequency is consistently 160 Hz when the drone is hovering without payload. A sudden shift in frequency is observed for all the weights when the payload is released, but more clearly for the heavier weights, which is expected. The fluctuations at times other than when the payload release occurred can be attributed to the wind causing the drone to stabilise itself. From the values shown in figure 12, the correlation between the dominant rotational frequency and payload weight can be determined, which is illustrated in figure 13.The upward trend in frequency as weight increases is evident. The reason for the frequency not increasing beyond 200 Hz is not fully known, but may reflect that the drone motors have reached maximum speed / thrust.

It should be noted that these results rely on identifying a relative change in frequency compared to the base frequency for any particular drone (e.g. 160 Hz for our S900). The absolute value of base frequency will vary with drone type and its particular configuration / payload which could only be determined by collecting a large dataset or having *a priori* knowledge of the motor speeds for a wide variety of drones. In practice,

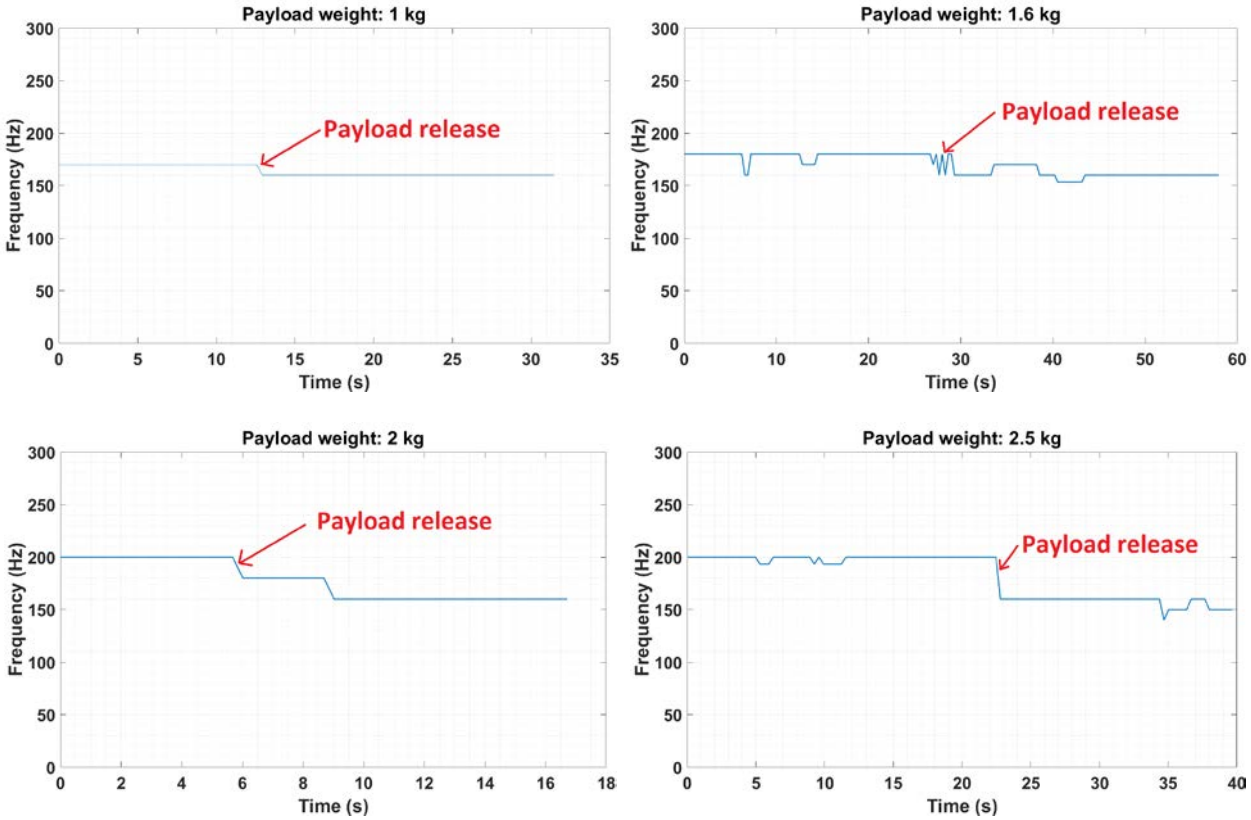

Figure 12: Trace of SVD based propeller dominant rotational frequency for S900 during payload release with payloads of 1 kg (top left), 1.6 kg (top right), 2 kg (bottom left), 2.5 kg (bottom right).

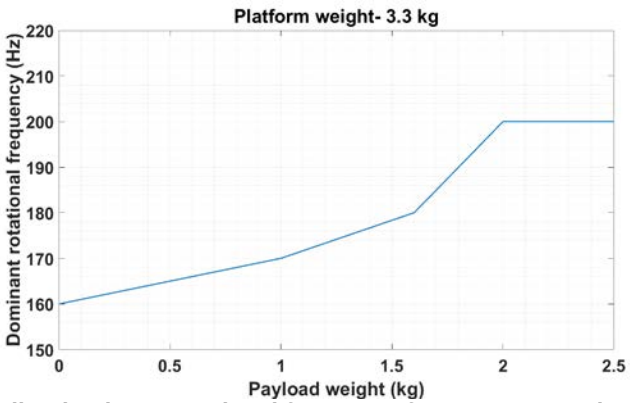

Figure 13: Propeller dominant rotational frequency for S900 vs attached payload weight.

this information is not likely be available, so we suggest it would be very difficult to robustly determine the presence of a payload from knowing the absolute rotation frequency. The sudden change in rotation frequency when a payload is dropped can be detected during continuous measurement but this may be too late to provide actionable information. The other main issues are the potential false alarms due to normal flight dynamics (wind or sudden acceleration) which exhibit similar changes in rotation frequency. We conclude that it would be very difficult to use any micro-Doppler based method to detect the presence of a payload on a drone with any reliability since the signatures are too similar to those of normal flight motions. This somewhat contradicts with the conclusion made in [7], which might be due to using different types of drones.

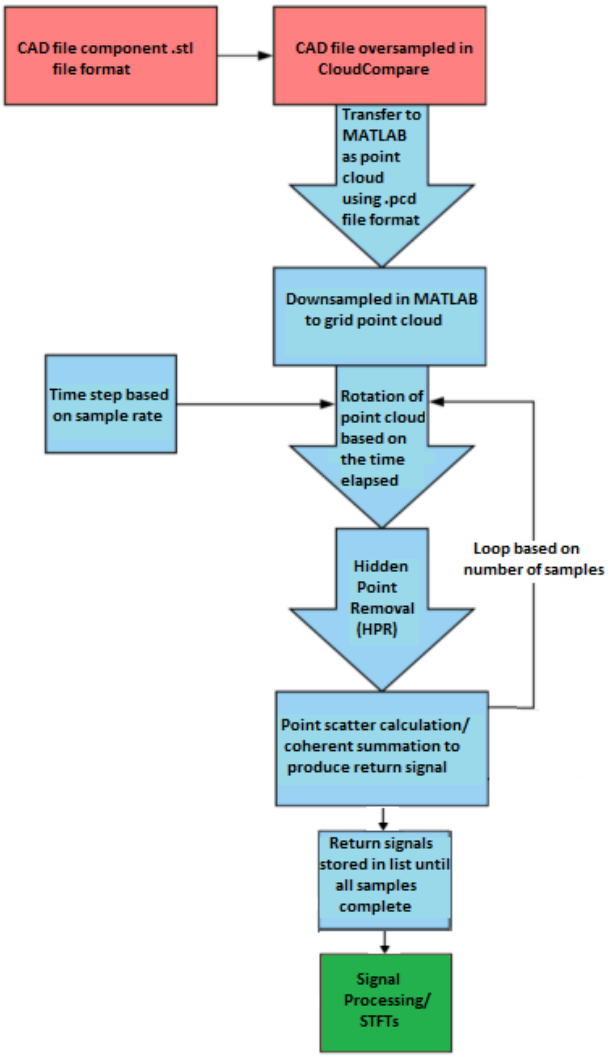

Figure 14: Flow chart of the radar micro-Doppler signature modelling process of the rotating components of drones.

For better analysis of the CW data, it is useful to model the micro-Doppler signatures imparted by the various components of the drone. This enables decomposition of the signal and investigation of the effect on components due to the presence of different types of payloads. Simulations were performed based on physically realistic structural models of the rotating components of the drone. The radar signal model of the target geometry accounted for line of sight shadowing effects (e.g.. a drone arm blocking the radar return from a blade at a certain angle). This approach provide more realistic micro-Doppler signatures, which provide a better understanding of the relationship between the signatures and the shape of the drone propeller blades and rotors.

Figure 14 illustrates the flowchart used of the whole process. For the drone component structure, CAD models were imported to the MATLAB environment for radar return signal modelling. Open source CAD models of blades, motors and arms of a DJI Phantom Standard 3 and DJI S900 were acquired from [20]. These two were chosen due to the availability of the experimental data, so that direct comparisons could be made. Separate CAD files were made for each component (motor, blades, clamps), allowing more flexibility in simulation. As seen in figure 14, point cloud files were then generated which were imported to MATLAB for processing. The Hidden Point Removal (HPR) algorithm used during the simulation was obtained from

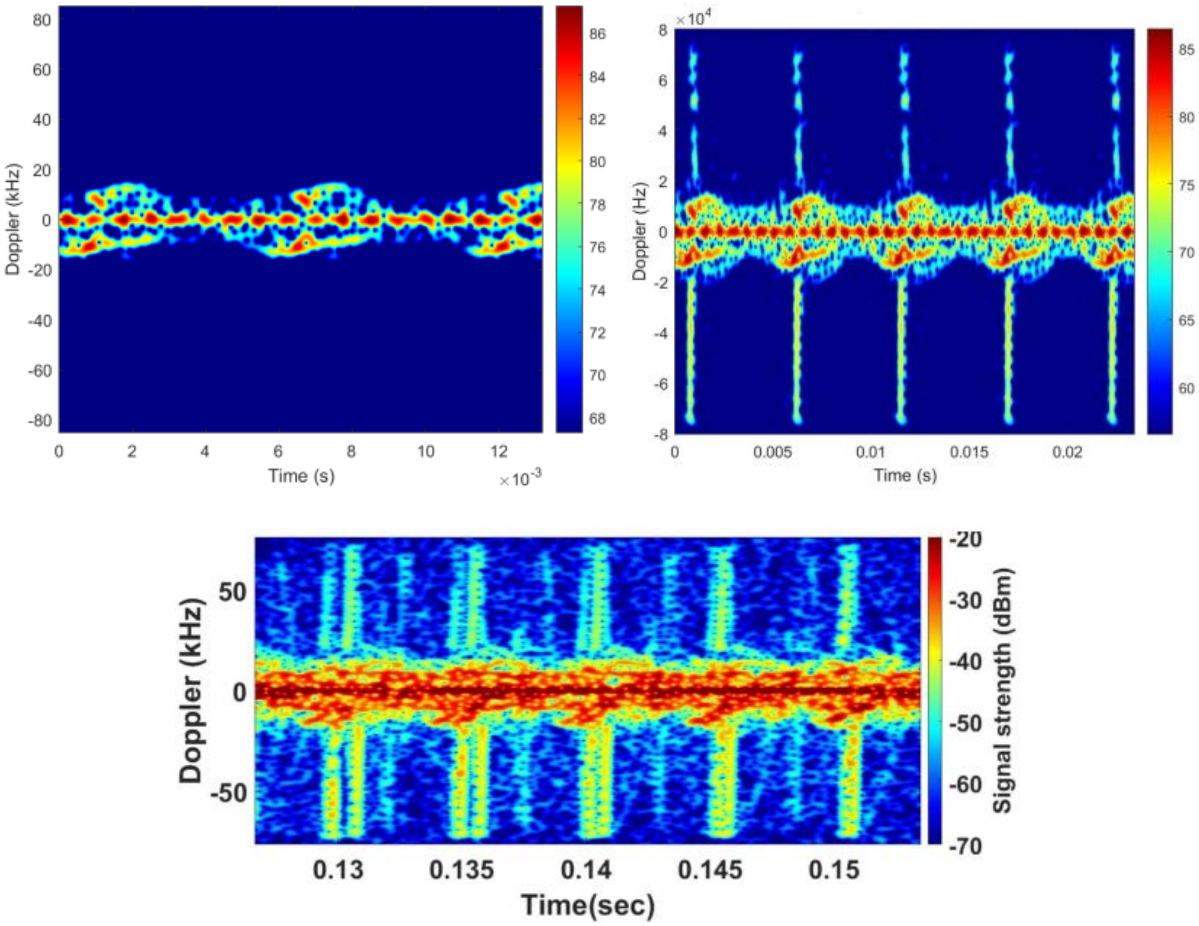

Figure 15: DJI S900 spectrogram plots- simulated spectrogram of the motor only (top left), simulated spectrogram of a motor, clamp and single blade combined (top right), spectrogram obtained from experimental trial with the S900 with 4 propellers flying at 20 m range (bottom).

[21]. This works with an operator that uses a projection method to reconstruct surfaces from a point cloud along with removing hidden points with high accuracy. The radar return signal simulation was then performed for 94 GHz centre frequency. To demonstrate the findings, figure 15 shows some example results, processed for DJI S900 which uses a motor and two blades attached with a clamp bar. Figure 15(top left) shows the simulated spectrogram of the S900 motor rotating without blades or clamp. In comparison, Figure 15(top right) shows the simulated spectrogram of an assembly of the S900 motor, clamp and a both blades, rotating at 100 Hz. The simulation parameters were intentionally chosen to be similar to the measured spectrogram shown in figure 15(bottom), which is processed from experimental data. Detailed good agreement is seen between the simulation and the experimental result, verifying the modelling method. The shape of the blade flashes and the slanted signatures from the motor are observed in both simulation and experimental results. Note the experimental data is for a flying S900 with 4 propellers so the spectrogram contains multiple sets of periodic blade flashes.

5.0 CONCLUSION

This study provides new insights into the radar signature characteristics of drones equipped with different malicious payloads. It has been demonstrated with simulation and subsequent experimental results that radar sensors can be used for the robust detection of certain threat payloads carried by drones. Three different scenarios have been considered and analysed in detail. It is shown that a millimetre-wave radar system (W-

band) is sensitive enough to detect small particulates dispersed from a crop spray drone, analogous to a biological/chemical weapon. The experimental trial results validated the predicted model well. Modelling of the recoil effect due to inertial forces has also shown a distinctive signature in the Doppler domain. It is demonstrated that the impulse generated by a gun will have a unique bulk Doppler signature which can be observed by both Fourier and wavelet transform analysis. The experimental trial results mimicking a drone-mounted gun recoil also validate the simulation. Finally, methods for detecting the presence of a heavy payload by tracking the change in the dominant rotation frequency of the propeller micro-Doppler signal have been discussed. It is confirmed that the dominant rotation frequency increases with increasing payload weight up to some limit. However, the absolute rotation rate, or sudden changes in its value, are not robust measures of the presence of a heavy payload since similar effects occur from normal flight dynamics e.g. caused by wind. However, some *a priori* knowledge based dataset or sensor fusion may be able to improve the classification accuracy in this case. For instance, a radio frequency (RF) sensor can potentially identify the drone model and the information then can be used by the classification algorithm along with the radar data.

Future work will consist of using the processed radar data to train classification algorithms for automatic threat payload detection. Neural network based algorithms (i.e. convolutional neural network) could be trained with the spectrogram plots to automatically identify the presence of particular threats associated with a drone. Additionally, more in-depth modelling of the CW micro-Doppler signatures of the drone components (i.e. multiple blades, variation with aspect angle etc.) will be made, accompanied by high resolution lab-based radar measurements for verification. These models can then be further modified with simulated threat scenarios. It is expected that this comprehensive characterisation of the micro-Doppler signatures will aid to better feature extraction performance for threat payload classification.

ACKNOWLEDGEMENTS

The authors acknowledge the funding received by the Army Research Laboratory under Cooperative Agreement Number: W911NF-19-2-0075. The views and conclusions contained in this document are those of the authors and should not be interpreted as representing the official policies, either expressed or implied, of the Army Research Laboratory or the U.S. Government.

REFERENCES

[1] "Small Drones Market Size Worth USD 22.55 Billion by 2026; Industry Driven by Recent Technological Advancements in Product Manufacturing, says Fortune Business Insights™." [Online]. Available: https://www.prnewswire.co.uk/news-releases/small-drones-market-size-worth-usd-22-55-billion-by-2026-industry-driven-by-recent-technological-advancements-in-product-manufacturing-says-fortune-business-insights-tm--840065149.html. [Accessed: 25-Feb-2020].

[2] "Warning Over Terrorist Attacks Using Drones Given By EU Security Chief." [Online]. Available: https://www.forbes.com/sites/zakdoffman/2019/08/04/europes-security-chief-issues-dire-warning-on-terrorist-threat-from-drones/#6da839877ae4. [Accessed: 25-Feb-2020].

[3] V. C. Chen, F. Li, S.-S. Ho, and H. Wechsler, "Analysis of micro-Doppler signatures," *IEE Proc. - Radar, Sonar Navig.*, vol. 150, no. 4, p. 271, 2003.

[4] V. C. Chen, *The micro-doppler effect in radar*. Artech House, 2011.

[5] J. de Wit, "Micro-Doppler analysis of small UAVs," in *2012 9th European Radar Conference : 31 October - 2 November 2012, Amsterdam, the Netherlands*, 2012, pp. 210–213.

[6] P. Molchanov, R. I. A. Harmanny, J. J. M. de Wit, K. Egiazarian, and J. Astola, "Classification of small UAVs and birds by micro-Doppler signatures," *Int. J. Microw. Wirel. Technol.*, vol. 6, no. 3–4, pp. 435–444, 2014.

[7] M. Ritchie, F. Fioranelli, H. Borrion, and H. Griffiths, "Classification of loaded/unloaded micro-drones using multistatic radar," *Electron. Lett.*, vol. 51, no. 22, pp. 1813–1815, Oct. 2015.

[8] S. Rahman and D. A. Robertson, "Coherent 24 GHz FMCW radar system for micro-Doppler studies," in *Proc. SPIE 10633, Radar Sensor Technology XXII*, 2018, no. 10633.

[9] D. A. Robertson, G. M. Brooker, and P. D. L. Beasley, "Very low-phase noise, coherent 94GHz radar for micro-Doppler and vibrometry studies," in *Proc. SPIE 9077, Radar Sensor Technology XVIII*, 2014, vol. 9077, p. 907719.

[10] "Drones of Mass Destruction: Drone Swarms and the Future of Nuclear, Chemical, and Biological Weapons." [Online]. Available: https://warontherocks.com/2019/02/drones-of-mass-destruction-drone-swarms-and-the-future-of-nuclear-chemical-and-biological-weapons/. [Accessed: 25-Feb-2020].

[11] "5L economic drone agriculture sprayer for beginner | drone agriculture sprayer | Joyance Tech." [Online].Available: http://www.wecanie.com/html/sprayer/products/low_price_drone_agriculture_sprayer_for_b.html. [Accessed: 25-Feb-2020].

[12] N. Currie, R. Hayes, and R. Trebits, *Millimeter-wave radar clutter*. Artech House, 1992.

[13] P. J. Speirs, "Millemetre-wave radar measurement of rain and volcanic ash," University of St Andrews, 2014.

[14] S. Rahman and D. A. Robertson, "In-flight RCS measurements of drones and birds at K-band and W-band," *IET Radar, Sonar Navig.*, vol. 13, no. 2, pp. 300–309, Sep. 2018.

[15] S. Rahman, D. A. Robertson, and M. A. Govoni, "Radar signatures of drones equipped with liquid spray payloads," in *2020 IEEE Radar Conference (RadarConf20)*, 2020, pp. 1-5, doi: 10.1109/RadarConf2043947.2020.9266374.

[16] M. J. Hall, "Effects of breech bolt movement on felt recoil of a gas-operated semi-automatic sporting gun," *Proc. Inst. Mech. Eng. Part P J. Sport. Eng. Technol.*, vol. 229, no. 3, pp. 159–168, Sep. 2015.

[17] S. Rahman and D. A. Robertson, "Radar micro-Doppler signatures of drones and birds at K-band and W-band," *Sci. Rep.*, vol. 8, no. 1, p. 17396, Dec. 2018.

[18] T. Thayaparan, S. Abrol, E. Riseborough, L. Stankovic, D. Lamothe, and G. Duff, "Analysis of radar micro-Doppler signatures from experimental helicopter and human data," *IET Radar, Sonar Navig.*, vol. 1, no. 4, p. 289, 2007.

[19] "'Recoil' entry in Wikipedia." [Online]. Available: https://en.wikipedia.org/wiki/Recoil. [Accessed: 25-Feb-2020].

[20] "GrabCAD: Design Community, CAD Library, 3D Printing Software." [Online]. Available:

https://grabcad.com/. [Accessed: 09-Feb-2021].

[21] S. Katz, A. Tal, and R. Basri, "Direct visibility of point sets," *ACM Trans. Graph.*, vol. 26, no. 3, p. 24, Jul. 2007.

AUTHOR BIOGRAPHIES

Samiur Rahman received the M.Sc. degree in Electrical Engineering from the Blekinge Institute of Technology, Sweden in 2010 and the Ph.D. degree from the University College London, UK in 2015. Since 2016, he has been a Research Fellow with the Millimetre-Wave and EPR group, University of St Andrews, UK.

Duncan A. Robertson received the B.Sc. (Hons.) degree in physics and electronics and the Ph.D. degree in millimetre-wave physics from the University of St Andrews, UK, in 1991 and 1994, respectively. He is currently a Principal Research Fellow with the Millimetre Wave and EPR Group, University of St Andrews, UK.

Adam M. Robertson received the M.Phys. (Hons.) degree in Physics from the University of St Andrews, UK, in 2020. His masters project, completed under the Millimetre Wave and EPR Group, University of St Andrews, focused on the characterisation of drones using millimetre wave radar simulations. He is currently a data scientist at InterGen, Edinburgh, UK.

Mark A. Govoni received the B.S.E. and M.S. degrees from Arizona State University, AZ, USA, in 2000 and 2001, respectively, and the Ph.D. from the Stevens Institute of Technology, NJ, USA in 2011. His research interests include radar signal processing, radar phenomenology, radar waveform design, and radar system optimization techniques.